

# LARGE-SCALE CLIMATE VARIABILITY AND CONNECTIONS WITH THE MIDDLE EAST IN PAST CENTURIES

MICHAEL E. MANN

*Department of Environmental Sciences, University of Virginia, Charlottesville, VA 22902, U.S.A.*

**Abstract.** We analyze reconstructions of large-scale surface temperature patterns in past centuries for insights into long-term climate change in the Middle and Near East. The temperature reconstructions, which have been described in detail previously, are based on calibration of widespread networks of high-resolution proxy and long instrumental/historical records against the 20th century global instrumental surface temperature record. We document the influence of several distinct patterns of large-scale surface temperature variation on Middle/Near East temperature ('MNET') in the region during past centuries. The dominant pattern of influence on interannual and decadal timescales is the North Atlantic Oscillation (NAO), exhibiting significant amplitude modulation on multidecadal and century timescales. Other patterns dominate multidecadal timescale MNET variations. The influence of such patterns, and recent decadal trends in the NAO, may mask the influence of anthropogenic climate change in the MNET region in recent decades.

## 1. Introduction

The Middle and Near East comprise a particularly climate-sensitive region from a societal standpoint. These regions are climatically stressed by extremes of heat, and limited water resources, which help create or exacerbate existing sociopolitical tensions. It is particularly vital, for these reasons, for us to understand those sources, be they natural or human, which govern climatic variability and change in this region of the world. Climate model simulations suggest that anthropogenic influences (greenhouse gas increases combined with aerosol increases) could lead to significant climatic change in this region during the next century. Temperature increases during all seasons, and shifting precipitation patterns are likely although their precise nature is far from certain (IPCC, 1996). Natural climate variability, however, is itself quite sizable in the region. While the El Niño/Southern Oscillation (ENSO) phenomenon, a dominant source of interannual climate variability over much of the globe, appears to have either an inconsistent (e.g., Rogers, 1984; Ropelewski and Halpert, 1987) or weak (e.g., Halpert and Ropelewski, 1992) influence on the climate of the region, there is recent evidence that the teleconnection of ENSO has indeed extended its reach into the Middle East in recent decades (Price et al., 1998). The North Atlantic Oscillation (NAO) atmospheric circulation pattern appears, by contrast, to exhibit a clear influence on the climate of the region on interannual and decadal timescales (see Cullen et al., 2002). Still longer-term, interdecadal-to-century-scale climate variations appear to impact the North At-



lantic and neighboring regions (e.g., Folland et al., 1984; Kushnir, 1994; Delworth et al., 1993, 1997; Mann and Park, 1994, 1996; Mann et al., 1995; Schlesinger and Ramankutty, 1994; Delworth and Mann, 2000). Such variations are difficult to confidently diagnose from the relatively short instrumental record, and deconvolving their influence from possible forced (e.g., anthropogenic) climate trends is difficult.

To distinguish between distinct natural and anthropogenic long-term climate influences, it is necessary to utilize longer-term archives of information. We report here an analysis of recent multiple-century reconstructions of global temperature patterns described in detail elsewhere (Mann et al., 1998 – henceforth, MBH98) for insights into long-term, large-scale influences on the climate of the Middle and Near East. We examine the histories of the dominant patterns of 20th century global temperature variability several centuries further back in time, providing a longer-term context for interpreting the influences of processes such as the NAO and multidecadal Atlantic climate modes, on the region. Insights into patterns of precipitation and drought in this region during the 20th century, and their relationship with the NAO (Cullen and deMenocal, 2002) are described elsewhere.

In Section 2, we describe the instrumental data used in this study. This includes a description of the instrumental surface temperature record and its leading patterns of variability, the North Atlantic Oscillation (NAO) index, including a surface temperature-based ('tNAO') alternative index of the phenomenon, the dataset of proxy climate indicators available for seasonal and annual climate reconstructions in past centuries, and an Middle East/Near East region surface temperature ('MNET') index used to describe surface temperature variations in that region. In Section 3, we describe the methods and data behind proxy-based reconstructions of the instrumental surface temperature record and the tNAO index in past centuries. In Section 4, we describe inferences from these reconstructions into climate changes in the Middle East over the past several centuries, and their relationships with large-scale patterns and trends. We summarize in Section 5 with some concluding remarks.

## 2. Instrumental Record

### 2.1. GRIDPOINT SURFACE TEMPERATURE RECORD

We consider the region of the globe with nearly continuous monthly sampling of surface temperatures during the twentieth-century. Specifically, we, as in MBH98, will consider of all land air and sea surface temperature gridpoint data from the East Anglia dataset (see Jones and Briffa, 1992; Jones et al., 1999) with nearly continuous monthly coverage during the period 1902–1980 (Figure 1). We also take note of a sparser subset of available nearly continuous gridpoint data available back to 1854, as shown.

Because of the importance of the Middle/Near East region in this study, we formulate an index of temperature variations in this region (the 'MNET' index) by

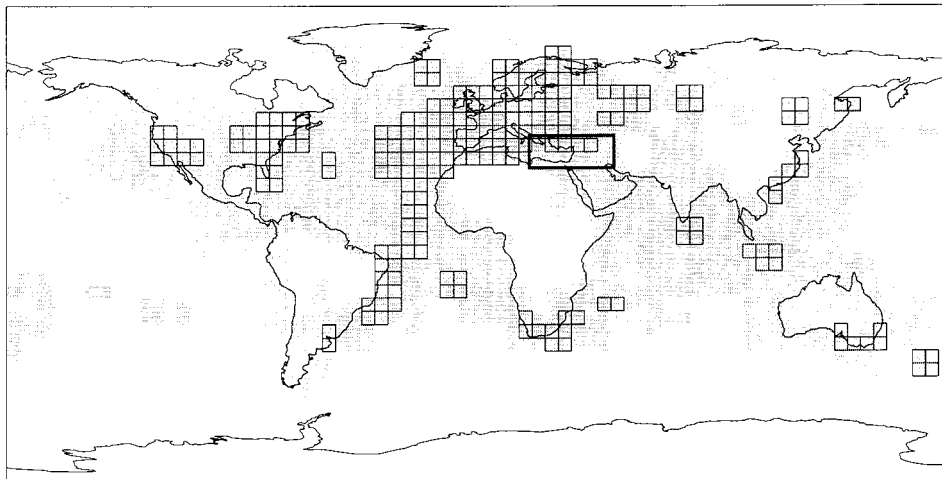


*Figure 1.* Distribution of instrumental temperature data used here and by Mann et al. (1998). Indicated by shading are the (1082) nearly continuous available land air/sea surface temperature gridpoint data available since 1902 onward. Squares indicate the subset of 219 gridpoints with nearly continuous records extending back to 1854. Northern Hemisphere (NH) mean temperature is estimated as areally weighted (i.e., cosine latitude) average over the domain north of the equator. The rectangle in the middle/near eastern region is the 'MNET' index region described in the text.

averaging the 12 surface temperatures gridpoints in this region (30–40° N latitude, 20–50° E longitude). A longer estimate of the MNET index is provided from the 4 gridpoints available back to 1854 (see Figure 1).

## 2.2. GLOBAL TEMPERATURE EIGENVECTORS

It is useful at this point to consider the patterns of the leading eigenvectors of the 20th century monthly surface temperature data, and how they relate to the MNET region. We consider specifically the 5 highest rank eigenvectors (Figure 2) which account for roughly one third of the total variance in the instrumental temperature record (see MBH98). Although mixing of signals is expected in a simple EOF decomposition, previous studies provide a remarkably simple physical interpretation of several of these leading eigenvectors.

The first eigenvector describes the dominant mode of global-mean temperature variation, while the second eigenvector describes the dominant ENSO-related pattern. MBH98 argue that the impact of secular external forcing is expressed largely in the 20th century trends in these two patterns. The first pattern, describing the large-scale warming trend, bears a resemblance to the generic greenhouse radiative forcing pattern (e.g., IPCC, 1996). The second pattern exhibits a negative La Niña-like trend also predicted as a dynamical response to greenhouse radiative forcing (Cane et al., 1997) as well as much of the residual ENSO variability. The third eigenvector expresses in large part climate variability associated with the North

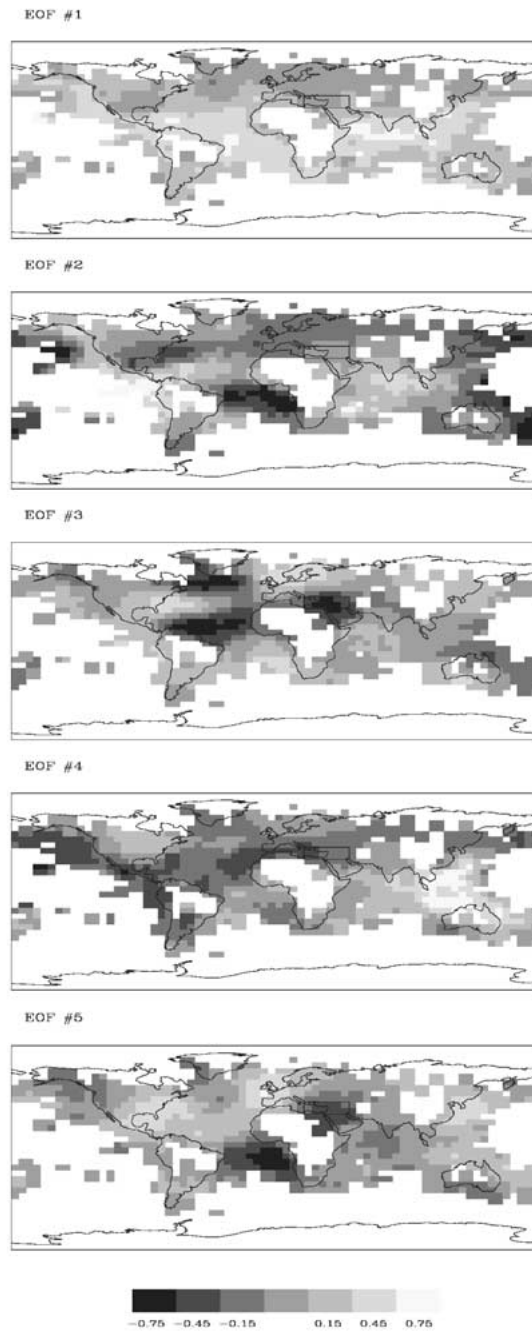


*Figure 2.* Empirical Orthogonal Functions (EOFs) for the five leading eigenvectors of the global temperature data from 1902–1980. The gridpoint areal weighting factor used in the PCA procedure has been removed from the EOFs so that relative magnitudes of temperature anomalies (indicated by grayscale) can be inferred from the patterns. Refer to MBH98 for color versions of the EOF patterns.

Table I

Correlations of first 5 PCs with MNET index during the 20th century (1902–1993). Also shown are correlations with Northern Hemisphere (NH) temperatures, and NAO, tNAO indices (see next section). Symbols note significance at the 90% (<sup>a</sup>), 95% (<sup>b</sup>), and 99% (boldfaced) levels based on a two-sided test taking into account serial correlation. Upper triangle (regular font) corresponds to annual mean values, while lower triangle (italics) corresponds to cold-season average values

	MNET	PC1	PC2	PC3	PC4	PC5	NH	pNAO	tNAO
MNET		0.23 <sup>b</sup>	-0.14	<b>-0.53</b>	-0.25 <sup>b</sup>	-0.17	<b>0.34</b>	<b>-0.45</b>	<b>-0.62</b>
PC1	<i>0.16</i>		-0.10	0.00	-0.09	0.05	<b>0.89</b>	-0.04	-0.14
PC2	<i>0.06</i>	<i>0.02</i>		0.05	0.03	0.10	-0.23 <sup>b</sup>	0.02	-0.21 <sup>a</sup>
PC3	<b>-0.56</b>	<i>0.10</i>	<i>-0.04</i>		-0.09	-0.26 <sup>b</sup>	-0.04	<b>0.47</b>	<b>0.57</b>
PC4	<i>-0.32<sup>b</sup></i>	<i>-0.11</i>	<i>-0.15</i>	<i>0.14</i>		-0.14	-0.29 <sup>b</sup>	0.13	0.13
PC5	<b>-0.44</b>	<i>0.01</i>	<i>-0.02</i>	<i>0.11</i>	<i>-0.10</i>		0.20 <sup>a</sup>	0.13	0.16
NH	<i>0.04</i>	<b>0.50</b>	<b>-0.33</b>	<i>0.30<sup>b</sup></i>	<i>-0.26<sup>b</sup></i>	<i>0.24<sup>b</sup></i>		0.04	-0.01
pNAO	<b>-0.48</b>	<i>-0.07</i>	<i>0.00</i>	<b>0.63</b>	<i>0.17</i>	<i>0.27<sup>b</sup></i>	<b>0.45</b>		<b>0.72</b>
tNAO	<b>-0.54</b>	<i>-0.16</i>	<i>-0.26<sup>b</sup></i>	<b>0.61</b>	<i>0.15</i>	<b>0.35</b>	<b>0.55</b>	<b>0.82</b>	

Atlantic Oscillation (NAO), while the 4th and 5th eigenvectors describe predominantly multidecadal variability in the Atlantic and Pacific basins and neighboring regions.

Table I shows the relationship between the time-evolution of these eigenvectors (the Principal Components or ‘PC’s) and the relationship between the MNET index and the subset of the 4 PCs (#s 1,3,4,5), which exhibit the strongest statistical relationship with the MNET index, is shown in Figure 3. The first eigenvector, describing the Northern Hemisphere/global warming trend this century, correlates well with the increase in MNET through the mid-20th century, but the relationship breaks down later in the 20th century. This breakdown appears to be associated with the influence of other patterns on the region, which oppose the trend, as discussed below. The overprint of natural variability on the MNET region is greatest during the cold season, and Northern Hemisphere mean temperature and MNET, while significantly correlated for annual-mean conditions, are not significantly correlated during the cold season.

The second eigenvector shows no significant relationship with MNET, consistent with the generally weak ENSO teleconnection to the region discussed earlier. However, the fourth eigenvector, which carries a more modest share of the ENSO signal, exhibits a more sizeable relationship with the MNET index, implying cold anomalies in southern Europe/Mediterranean region in association with cold-phase (La Niña) ENSO conditions, described in previous studies (Halpert and Ropelewski, 1992). The pattern further, however, suggests an extension of ENSO influence into the MNET region. Indeed, the substantial recent decadal trend in this

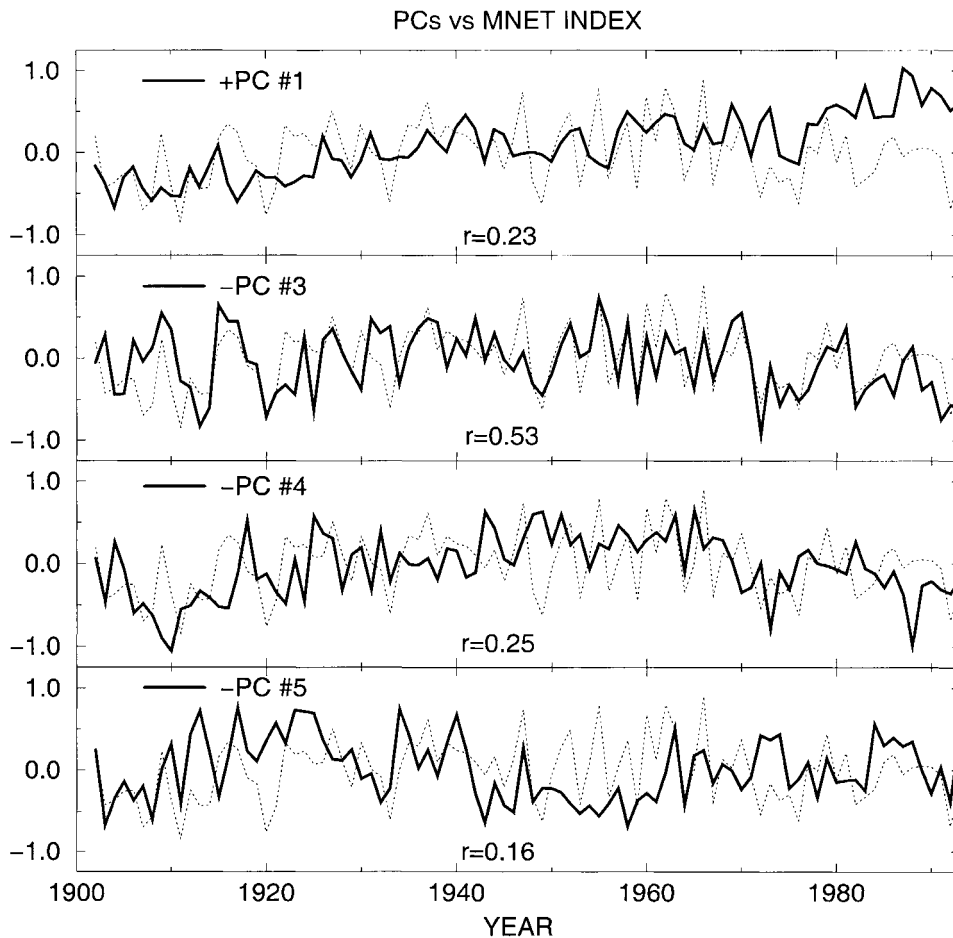


Figure 3. Principal Components (PCs) for the leaving eigenvectors (#s 1,3,4,5) which exhibit a statistically significant relationship with the MNET temperature index. Signs are reversed for PCs #3,4,5 to yield positive correlations (indicated in plot) with MNET index.

pattern over the past few decades (see Figure 3), apparently associated with multidecadal timescale modulation of ENSO by Atlantic processes (see Rajagopalan et al., 1998), may lead to the previously noted non-stationarity of ENSO teleconnections in the Middle East (Ropelewski and Halpert, 1987; Price et al., 1998 – the authors note evidence of an increase in recent decades in the influence of El Niño on precipitation patterns in the middle east). Such nonstationarity appears, indeed, to be reflected in the multidecadal and century-scale modulation of the relative prominence of distinct ENSO temperature teleconnection patterns (see Cole and Cook, 1998; Mann et al., 2000a).

The third eigenvector, as discussed in more detail below, is largely associated with the NAO, and resolves the largest fraction of variance in the MNET index

(28% for annual mean, 31% for cold season). A decadal-scale positive trend in this eigenvector (see Figure 3, note sign convention), is associated with a recent shift towards more positive NAO conditions (see Hurrell, 1995), which favor (see below) cooling in the MNET region. This recent shift, which has also been speculated as potentially anthropogenic in nature (Shindell et al., 1999) tends, along with other patterns discussed below, to obscure any warming associated with the global-scale warming pattern described by the first eigenvector.

The fifth eigenvector (in quadrature, with the fourth eigenvector discussed above) describes a temporally evolving multidecadal pattern centered in the Atlantic which may arise from organized variability in the North Atlantic thermohaline circulation, and associated changes in North Atlantic SST and Northern Hemisphere atmospheric circulation (Delworth and Mann, 2000). While this pattern exhibit only a marginal annual-mean MNET influence, it describes roughly 20% of the MNET variance during the cold season, when it is most active, which is similar in magnitude to that described by the NAO-related third eigenvector.

It should be noted (see Table I) that the annual and seasonal PCs need not be orthogonal because they are computed as the annual means of the PCs of the *monthly* surface temperature data (see MBH98), that latter indeed being orthogonal. Nonetheless, the correlated variance annual and seasonal PCs is, with only a few exceptions, statistically insignificant (see Table I), so that the eigenvectors can typically be considered statistically independent on a seasonal or annual basis.

### 2.3. THE NORTH ATLANTIC OSCILLATION (NAO)

Because the NAO is such an important source of interannual climate variability in the region of interest, it is worthwhile to examine its influence more closely. To favor interpretations of NAO-related patterns from proxy-based temperature reconstructions described later, it is worthwhile at this point to formulate an NAO index in terms of the large-scale surface temperature field. Following previous workers, we do so through using a screening regression approach (Cook et al., 1998; see also D'Arrigo et al., 1997; Cullen et al., 2002). We seek, from such an analysis, to establish an optimal statistical relationship between the conventional pressure-based NAO index (which we term 'pNAO') and the gridpoint land air/sea surface temperature data described earlier (see Figure 4). The cold-season (Oct–Mar) pNAO index of Jones et al. (1997) is used for calibration against both the annual-mean and cold-season gridpoint surface temperature data to form both a cold-season and annual temperature-based 'tNAO' index. PC #3, as discussed earlier, exhibits the dominant relationship with the pNAO among the five highest rank eigenvectors (see Table I). The variance of the atmospheric pNAO resolved by the tNAO (Table I) is approximately 50% for the annual mean tNAO (see Figure 5) and 67% for the cold-season tNAO. Henceforth, we will only refer to the more meaningful, cold-season tNAO.

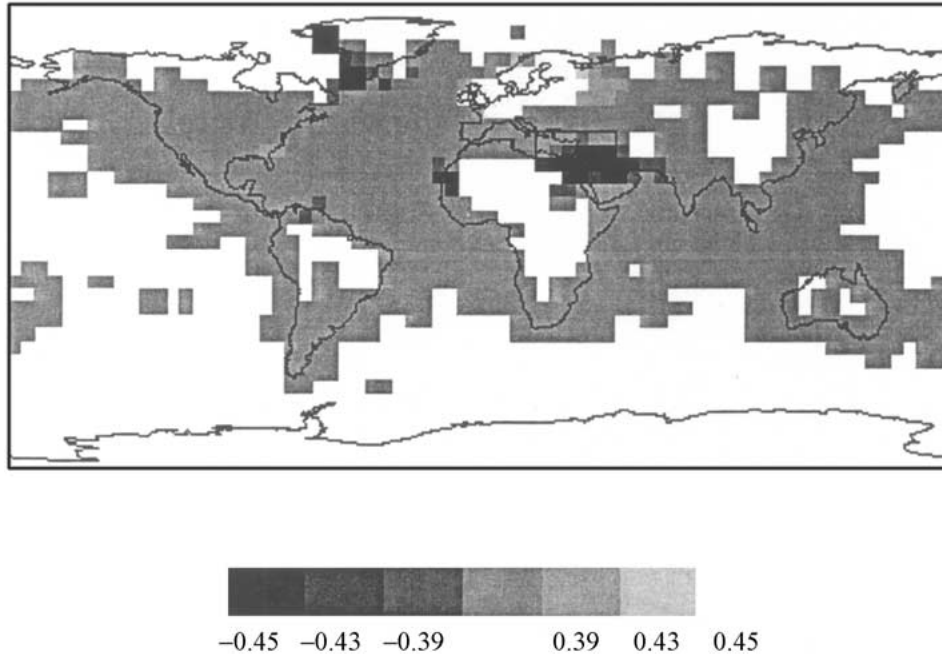


Figure 4. Correlation pattern of the cold-season (Oct.–Mar.) slp-based NAO index ('pNAO') against land air and SST gridpoint data from 1902–1993. The tNAO index discussed in the text is defined by a screening regression, using a standardized composite of all temperature gridpoints exhibiting a greater than 95% significant two-sided correlation (absolute value  $r = 0.39$ ) with the NAO index. The grayscale thresholds correspond to 95% ( $r = 0.39$ ), 98% ( $r = 0.42$ ) and 99% ( $r = 0.45$ ) two-sided significance levels.

The recent prolonged positive phase of the NAO discussed earlier is associated with a very similar shift in the tNAO index and, as indicated by Figure 3, such a shift is associated with cooling in the Middle/Near east. If, as suggested recently (Hurrell, 1995) recent extratropical cold-season global warming is associated with a positive shift in the NAO, we might expect trends in MNET to continue to oppose those in Northern Hemisphere cold-season temperatures. Such a relationship (see Table I) between cold-season hemispheric mean temperature and both the pNAO and tNAO cold-season index is supported in our analysis. It is noteworthy, however, that the *annual*, areally-weighted Northern Hemisphere mean temperature series used as an index of global warming and a detection variable for external climate forcing (see MBH98) shows no significant statistical relationship with the NAO index during the 20th century.

Figure 6 compares the spectra of the tNAO and pNAO indices during their period of overlap. Both indices capture the enhanced 8–9 year variance peak of the 20th century. The reconstructed tNAO index exhibits a similar spectrum to the instrumental tNAO index, though there is an absence of resolved variance at inter-annual timescales of 5–7 years, and somewhat enhanced decadal-scale variability

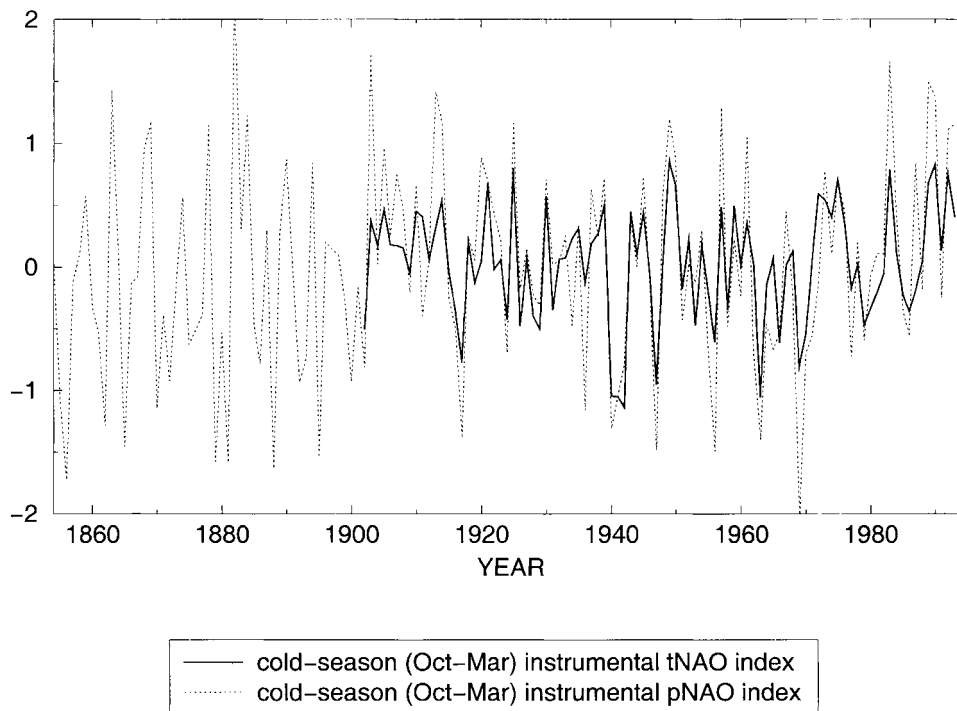


Figure 5. Comparison of tNAO index defined in text with cold-season instrumental pNAO index.

in the reconstructed index relative to the instrumental index. The redder spectrum, and greater decadal-scale variability, of the tNAO index is consistent with the greater thermal inertia of sea surface temperatures, and the distinct decadal-scale variability of Atlantic SST (Mann and Park, 1994; Mehta and Delworth, 1995; Chang et al., 1997; Tourre et al., 1998), which is suppressed in atmospheric circulation measures. From the point of view of the ocean as the carrier of the most significant sources of low-frequency variability, the tNAO index might be considered a preferable alternative (see Cullen et al., 2002).

### 3. Paleoclimate Reconstructions

#### 3.1. PROXY CLIMATE DATA

'Multiproxy' networks consisting of diverse proxy indicators have been used in recent studies to describe large-scale climate changes in past centuries (Bradley and Jones, 1992; Hughes and Diaz, 1994; Mann et al., 1995; Overpeck et al., 1997; Jones et al., 1998). Mann and coworkers have recently used such multiproxy networks to reconstruct annual (see MBH98; Mann et al., 1998, 1999, 2000a) and seasonal (Mann et al., 2000b) global surface temperature patterns in past cen-

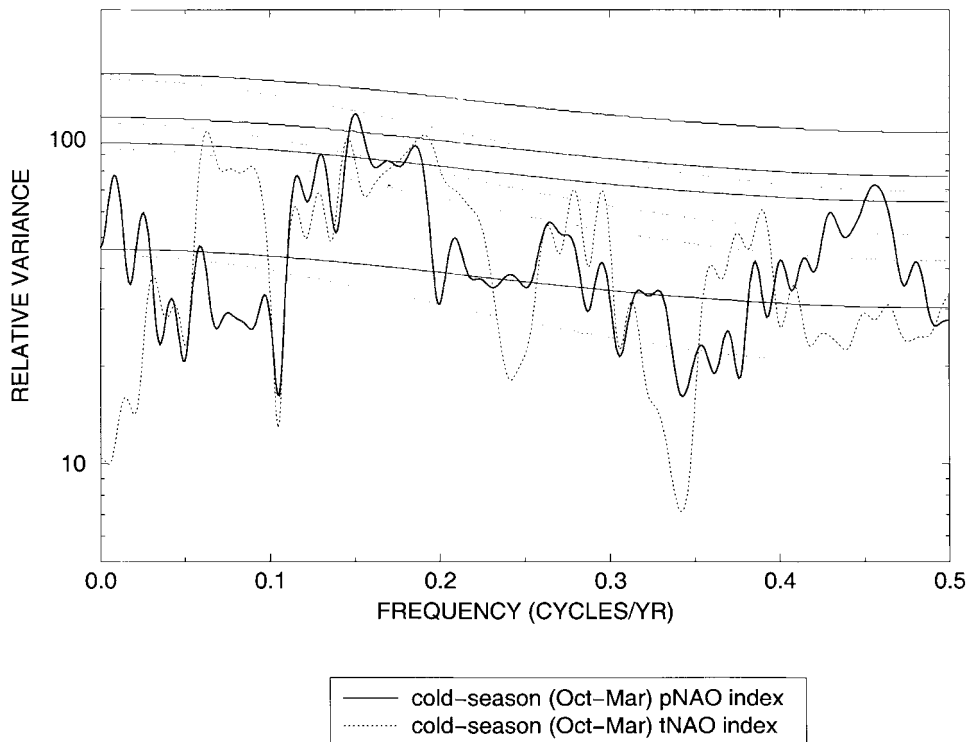


*Figure 6.* Comparison of spectra of cold-season pNAO (solid) and tNAO (dashed) index during common 1902–1980 interval. Median and 90%, 95%, 99% confidence levels relative to the null hypothesis of red noise are shown by the smooth curves for both the pNAO (solid) and tNAO (dashed) indices. Owing to its relatively reduced variance, the mean amplitude of the tNAO index spectra has been rescaled to coincide with that of the pNAO. Here, as in future similar figures, the spectra shown are based on the multitaper spectral estimation procedure of Mann and Lees (1996), invoking robust estimation of the red noise background and associated confidence levels.

turies. The multiproxy network used by Mann et al. consist of a combination of annually-resolved proxy indicators (dendroclimatic, coral, and ice core records) combined with the few long available historical or instrumental climate records. While more than 400 tree ring records are available (see MBH98, supplementary information), MBH98 create a more homogenous ‘multiproxy’ network by replacing dense regional sets of dendroclimatic indicators with their fewer significant principal components, leading to a network of 112 indicators available back to 1820 (Figure 7). This network becomes increasingly sparse back in time. In this study, we consider only the period dating back to 1750 during which the available proxy data network is, as described below, adequate to usefully resolve the regional patterns of interest in this study. Skillful reconstruction of Northern Hemisphere mean temperature are nonetheless possible, albeit with expanded uncertainties, considerably farther back in time, to about AD 1000 (Mann et al., 1999).

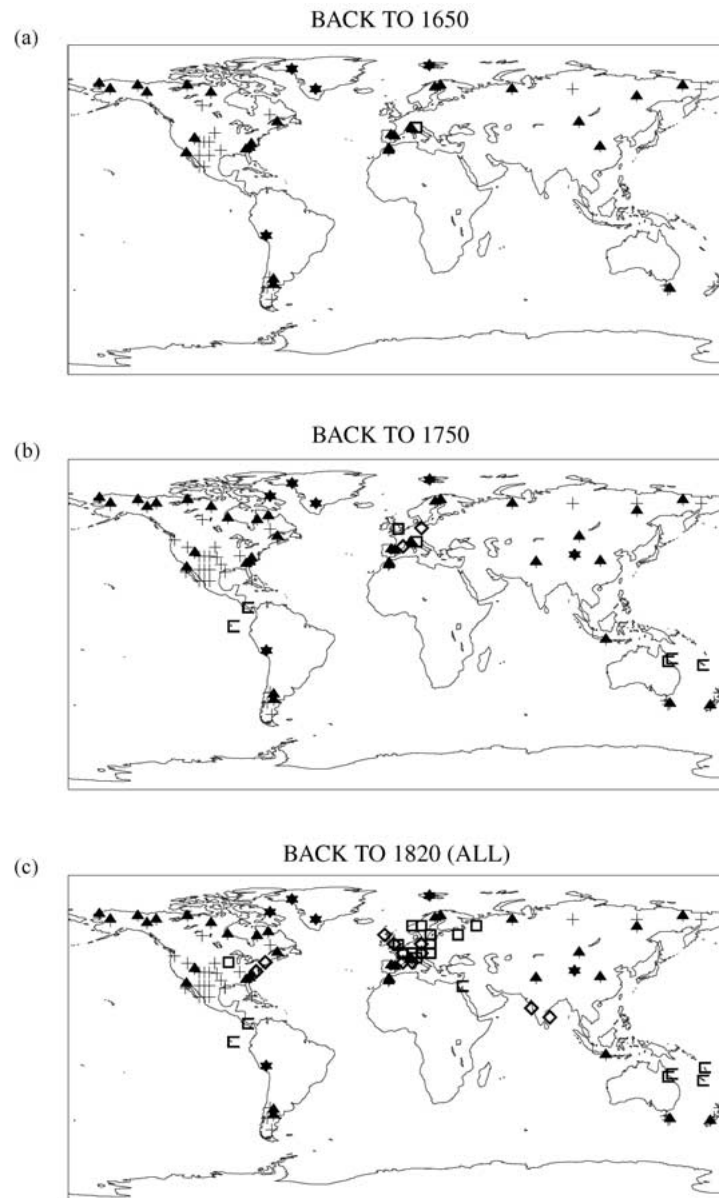


*Figure 7.* Distribution of multiproxy network used in this study back to (a) 1650, (b) 1750, and (c) 1820 (all proxy indicators). Squares denote historical and instrumental temperature records, diamonds denote instrument precipitation records, umbrella or ‘tree’ symbols denote dendroclimatic indicators, and ‘C’ symbols indicate corals. Groups of ‘+’ symbols indicate principal components of dense tree-ring subnetworks, with the number of such symbols indicating the number of retained principal components. Further details about the proxy data are found in MBH98. Note the considerably more widespread coverage available after 1750, corresponding to the period studied here.

### 3.2. RECONSTRUCTIONS: CALIBRATION AND VERIFICATION

#### *Large-Scale Temperature Patterns*

The method of climate reconstruction, as described in detail elsewhere (MBH98; Mann et al., 1999, 2000a,b), is based on the calibration of the proxy climate indicators shown in Figure 7 against the leading eigenvectors of the twentieth century (1902–1980) monthly instrumental surface temperature data (the first 5 of which are shown in Figure 2). The 1980 cutoff year for the calibration period corresponds to a dramatic dropoff in the available proxy indicators (of the 112 indicators available through 1980, only 19 are available through 1985). The reconstructions are ‘verified’ by comparing them against an independent set of instrumental surface temperature measurements from 1854–1901 held back from the calibration period for statistical cross-validation. The fraction of total variance resolved (for which we use the term ‘ $\beta$ ’ – see MBH98 for further discussion) is calculated during both the calibration and verification intervals (the reader should note that, unlike the case for simple linear regression,  $\beta$  is not identical to the squared correlation coefficient  $r^2$  during either the calibration or verification period, although  $\beta$  and  $r^2$  typically have similar values during the calibration period. A similarity of the verification period value of  $\beta$  to the calibration period value is an indication or ‘verification’ of the reliability of the reconstructions back in time.

For the period after AD 1820, when all 112 indicators shown in Figure 7 are available, it was possible to skillfully reconstruct 11 eigenvectors (i.e., 11 PCs of the instrumental temperature record) in the annual-mean pattern reconstructions, resolving roughly 80% of the Northern Hemisphere temperature variance in calibration and verifying a similar proportion of 70% of the variance during the verification period. The calibrated/cross-validated variance resolved in the full spatial temperature field is somewhat more modest (20–30%). The number of patterns that can be skillfully reconstructed decreases back in time, as the dataset becomes sparser. Back to 1750, 89 indicators are available, 8 eigenvectors are calibrated, 65–75% of the Northern Hemisphere mean temperature series is resolved in calibration/verification, and 10–20% of the total spatial variance is resolved. Back to 1700, 74 records are available, 5 eigenvectors are resolved, 60–70% of the Northern Hemisphere mean series, and roughly 10% of the total spatial variance are resolved in calibration/verification. We focus here on the reconstructed temperature patterns back through 1750, for which meaningful inferences in to the Atlantic and neighboring regions are possible. Back through 1750, roughly 25–30% of the instrumental temperature variance is captured during the calibration/verification intervals in the Atlantic and neighboring continental regions (see Figure 3 in MBH98). The variance resolved in warm and cold-season half-year reconstructions is somewhat less than that cited above for the annual-mean reconstructions (Mann et al., 2000b).

### *MNET Index*

We focus here on the results of the calibration and verification results for the MNET index used to characterize temperature variations in the Middle/Near East. As shown in MBH98 (Figure 3 therein), the calibration resolved variance based on the full multiproxy network (available back to 182) is uniformly high in this region ( $>15\%$  for each of the 12 gridpoints in the MNET region), with a resolved variance of 40% ( $\beta = 0.40$ ) for the MNET index itself. The calibrated variance decreases slightly back in time, with  $\beta = 0.3$  for the network available back to 1760, and  $\beta = 0.2$  for the network available back to 1750. Reconstructions prior to 1750 no longer resolve the essential 3rd PC, and the resolved MNET variance falls below  $\beta = 0.1$ , rendering the reconstructions useless for the regional inferences of interest.

The verification period explained variance (see also MBH98, Figure 3), however, shows far less consistency among the 4 gridpoints available in the region, with 2 gridpoints exhibiting negative values of  $\beta$ , and 1 gridpoint exhibiting a value  $\beta > 0.15$ . The verification resolved variance for the annual-mean MNET index based on these 4 gridpoints ( $\beta = 0.04$ ) is statistically significant, and exceeds the skill of climatology. It is, however, quite modest compared to the calibration period value, and considerably smaller than the verification resolved variance scores in many other regions. For the cold-season MNET reconstruction, the resolved variance is lower ( $\beta = 0.26$  in calibration,  $\beta = 0.0$  in verification).

The reconstructed annual-mean MNET index (based on the average of the annual-mean pattern reconstructions over all 12 gridpoints) is compared to the instrumental index based on both the dense sampling (all 12 gridpoints) available after 1902, and the sparse (4 gridpoints) sampling available during the 1854–1901 verification period (Figure 8). Also shown is the comparison of the 4 gridpoints available within the MNET region back to 1854. The 4 gridpoints track almost identically during the mid and late 20th century, and provide an excellent approximation to the full MNET index during that period. Considerable discrepancies are evident in the comparison between gridpoints prior to that interval however (the breakdown appears particularly marked prior to 1871, although notable discrepancies continue into the 20th century).

Possible sources of bias in the gridpoint temperature data have been discussed elsewhere in detail (e.g., Jones and Briffa, 1992), and we find it possible that such systematic sources of error compromise the quality of the MNET index prior to the mid-20th century. An alternative cross-validation exercise based on an independent reconstruction of the MNET index during the decade 1971–1980, based on calibration during the interval 1902–1970 period, yields a verification resolved variance (36%) similar to the calibrated value, giving us more confidence in the skillfulness of the MNET reconstructions. However, our inability to provide a convincing pre-20th century verification of the MNET index suggests that the current MNET reconstruction must in any case be interpreted cautiously.

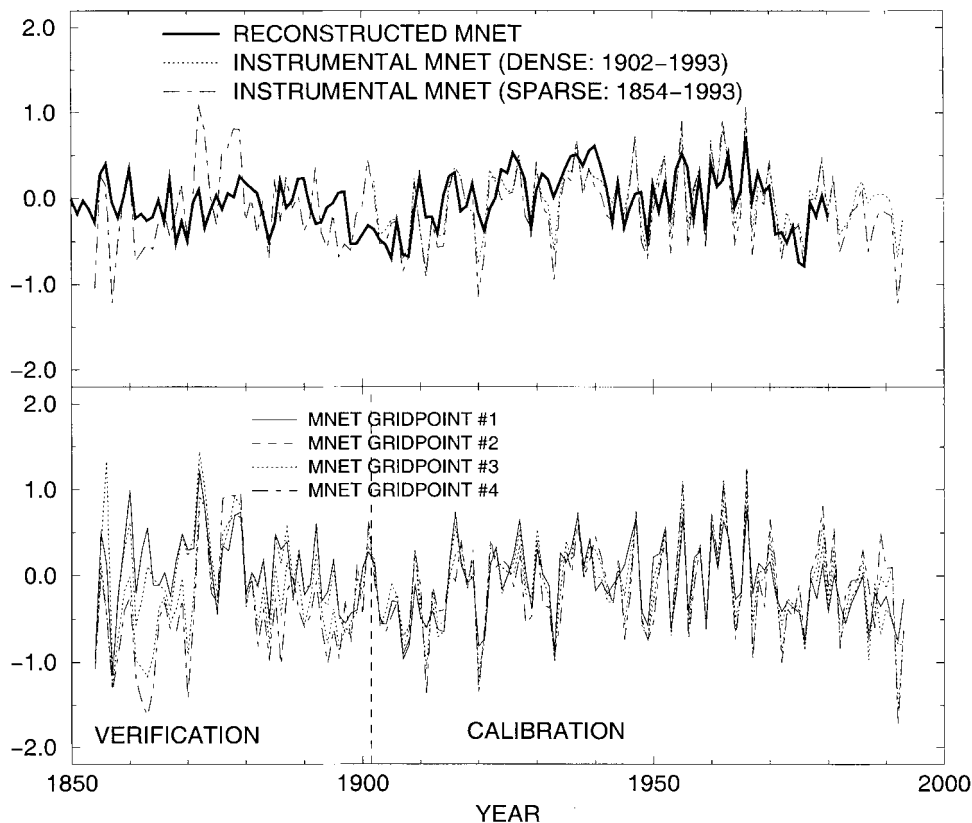


Figure 8. MNET index (a) comparison of reconstructed and actual instrumental MNET index during calibration interval (b) comparison of the 4 gridpoints available in the MNET region during the verification period during both the calibration and verification period.

### *tNAO*

The reconstructed cold-season *tNAO* index is compared with the instrumental *tNAO* and *pNAO* index during the calibration and verification intervals in Figure 9. The calibration resolved variance of the reconstructed *tNAO* is  $\beta = 0.57$  against the *tNAO* and  $\beta = 0.35$  against the *pNAO*. During the verification period, wherein an instrumental *tNAO* index is not available for comparison, the verification against the instrumental *pNAO* index is  $\beta = 0.26$ . This is equivalent to a value of at least  $\beta = 0.39$  against the *tNAO*, given the 67% shared variance between the instrumental *tNAO* and *pNAO* (i.e., Figure 5). These diagnostics suggest that the cold-season *tNAO* reconstruction resolves somewhere between 40–60% of the true *tNAO* variance.

The *tNAO* reconstruction also captures reasonably well the frequency-domain features of the instrumental *tNAO* index during the common calibration interval (Figure 10). Both the instrumental index and reconstruction shows enhanced variance at decadal timescales (8–25 years). The reconstruction, however, exhibits

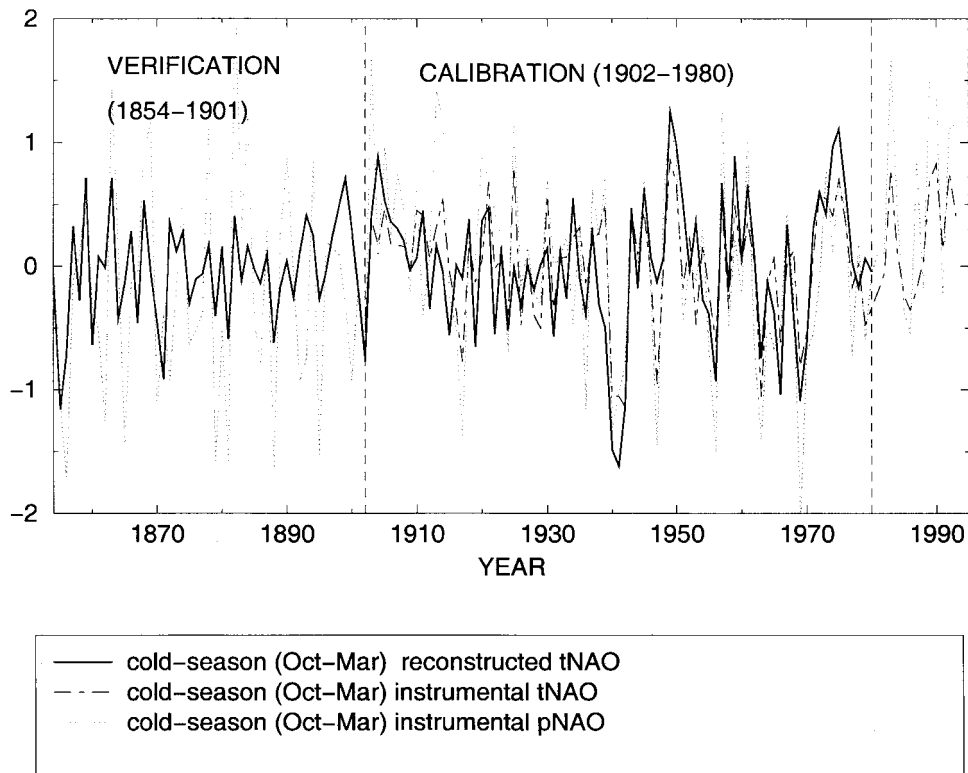
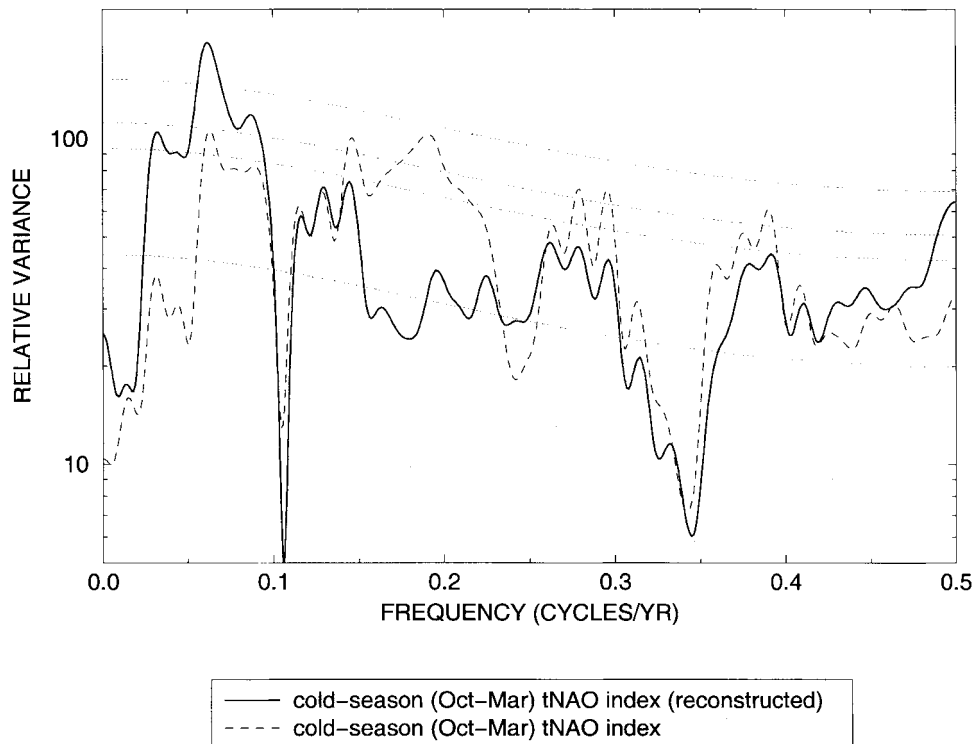


Figure 9. Comparison of tNAO index defined in text with cold-season instrumental SLP-based NAO index showing (a) instrumental indices and (b) reconstructed tNAO index along with instrumental NAO during calibration and verification subintervals (separated by the vertical dashed line).

too high amplitude variability at bidecadal timescales, and too little amplitude at roughly 4–7 year interannual timescales. These differences are, however, consistent with random calibration uncertainties, rather than systematic frequency-domain biases in the reconstruction.

Alternative proxy-based reconstructions of the winter (DJFM) NAO index have been attempted from dendroclimatic (D'Arrigo et al., 1993; Cook et al., 1998) and ice accumulation data (Appenzeller et al., 1998), while extensions of the instrumental NAO index back to the early 19th century are described by Jones et al. (1997). The merit of combining alternative reconstructions of the NAO index with complimentary statistical attributes into a single, more robust proxy-based NAO reconstruction has been discussed elsewhere (Cullen et al., 2002).



*Figure 10.* Reconstructed tNAO vs. instrumental tNAO spectrum during the 1902–1980 calibration interval. The median, 90%, 95%, and 99% confidence levels relative to the null hypothesis of red noise are shown by the dashed curves. The spectrum and confidence intervals are estimated by the method of Mann and Lees (1996).

#### 4. Variations in Past Centuries: Middle East and Large-Scale Connections

Though none of the records in the multiproxy network lie within the Middle/Near East region of interest (see Figure 2), inferences into climate changes in this region are possible, as shown in the previous section, because of the way in which our method optimally interpolates information from sparse surrounding proxy records. Past studies have looked at local dendroclimatic evidence for climate change during the past few centuries for southwestern Europe and northwestern Africa (Serre-Bachet et al., 1992), and coral isotopic evidence for climate changes in the Red Sea (Heiss, 1994) – indeed, these latter data are used in the present study. Considerable spatial variability is evident in surrounding regions in other studies. For example, Serre-Bachet et al. (1992) suggests that a ‘Little Ice Age’ appears in Southern Europe, but is not apparent in the western Mediterranean. We know of no systematic proxy-based studies, however, of climate changes in past centuries in the Middle/Near East region. It is thus worth investigating apparent such changes from the surface temperature reconstructions described earlier.

Table II

Correlations of RPCs #1,2,3,5 with NAO, tNAO and MNET indices during the full reconstruction (top: 1760–1980) and pre-calibration only (bottom: 1760–1901) periods. Symbols note two-sided significance at the 90% (<sup>a</sup>), 95% (<sup>b</sup>), 99% (boldfaced) levels. Upper triangle (regular font) corresponds to annual mean values, while lower triangle (italics) corresponds to cold-season average values

	MNET	PC1	PC2	PC3	PC4	PC5	NH	tNAO
<i>1760–1980 (full reconstruction)</i>								
MNET		<b>0.37</b>	-0.17 <sup>a</sup>	<b>-0.55</b>	<b>-0.24</b>	-0.22 <sup>b</sup>	<b>0.38</b>	<b>-0.59</b>
PC1	<b>0.24</b>		-0.11	-0.16 <sup>a</sup>	<b>-0.28</b>	0.06	<b>0.87</b>	<b>-0.33</b>
PC2	<i>-0.06</i>	<i>0.18<sup>a</sup></i>		0.05	0.09	0.20 <sup>a</sup>	<b>-0.31</b>	-0.13
PC3	<b>-0.73</b>	<i>-0.09</i>	<i>-0.03</i>		-0.16	<b>-0.44</b>	-0.10	<b>0.71</b>
PC4	<b>-0.32</b>	<i>-0.20<sup>a</sup></i>	<i>0.17<sup>a</sup></i>	<i>0.01</i>		-0.03	<b>-0.51</b>	0.07
PC5	<b>-0.50</b>	<i>-0.08</i>	<i>0.16<sup>a</sup></i>	<i>-0.01</i>	<i>0.07</i>		0.15	-0.02
NH	<b>0.36</b>	<b>0.89</b>	-0.11	-0.17 <sup>a</sup>	<b>-0.48</b>	0.03		-0.11
tNAO	<b>-0.72</b>	<b>-0.42</b>	<b>-0.45</b>	<b>0.64</b>	<i>0.00</i>	<b>0.37</b>	<b>-0.24</b>	
<i>1760–1901 (pre-calibration period)</i>								
MNET		<b>0.35</b>	-0.09	<b>-0.59</b>	-0.10	-0.11	0.25 <sup>b</sup>	<b>-0.61</b>
PC1	<i>0.00</i>		0.26 <sup>b</sup>	-0.23 <sup>a</sup>	0.10	0.16	<b>0.82</b>	-0.27 <sup>b</sup>
PC2	<i>0.05</i>	<b>0.65</b>		0.05	0.09	0.20 <sup>a</sup>	<b>-0.31</b>	-0.13
PC3	<b>-0.76</b>	<i>-0.10</i>	<i>-0.04</i>		-0.26 <sup>b</sup>	<b>-0.50</b>	-0.05	<b>0.76</b>
PC4	<i>-0.09</i>	<i>0.06</i>	<i>-0.09</i>	<i>-0.13</i>		-0.01	-0.19 <sup>a</sup>	-0.13
PC5	<b>-0.43</b>	<i>0.10</i>	<i>0.20<sup>a</sup></i>	<i>-0.13</i>	<i>0.06</i>		0.27 <sup>b</sup>	-0.06
NH	<i>0.10</i>	<b>0.89</b>	<b>0.51</b>	-0.25 <sup>b</sup>	-0.20 <sup>a</sup>	0.27 <sup>b</sup>		0.12
tNAO	<b>-0.72</b>	<b>-0.52</b>	<b>-0.52</b>	<b>0.62</b>	<i>-0.09</i>	0.26 <sup>b</sup>	<b>-0.39</b>	

Table II indicates the statistical relationships between the first five reconstructed PCs for both for the full period of reconstruction (1760–1980) and only the pre-calibration (1760–1901) period. The relationships between the MNET and reconstructed PCs #1,3,4,5 are shown in Figure 11. The period 1920–1960 is the warmest reconstructed interval for the MNET region, though confidence is the amplitude of past anomalies is limited by the 60% unresolved calibration variance. The downward shift during the 1980s is the largest observed, associated with the fairly dramatic decadal upturn of the NAO in the 1980s. The decade from 1898 to 1908 is the coldest in the reconstruction. Even taking into account the slightly decreased resolved variance in the reconstructed MNET index prior to 1780, the 20th century appears to exhibit more extreme behavior. However, the substantial uncertainties, and limitations for verifying the reconstructions in the region prior to the calibration period suggests caution in this conclusion.

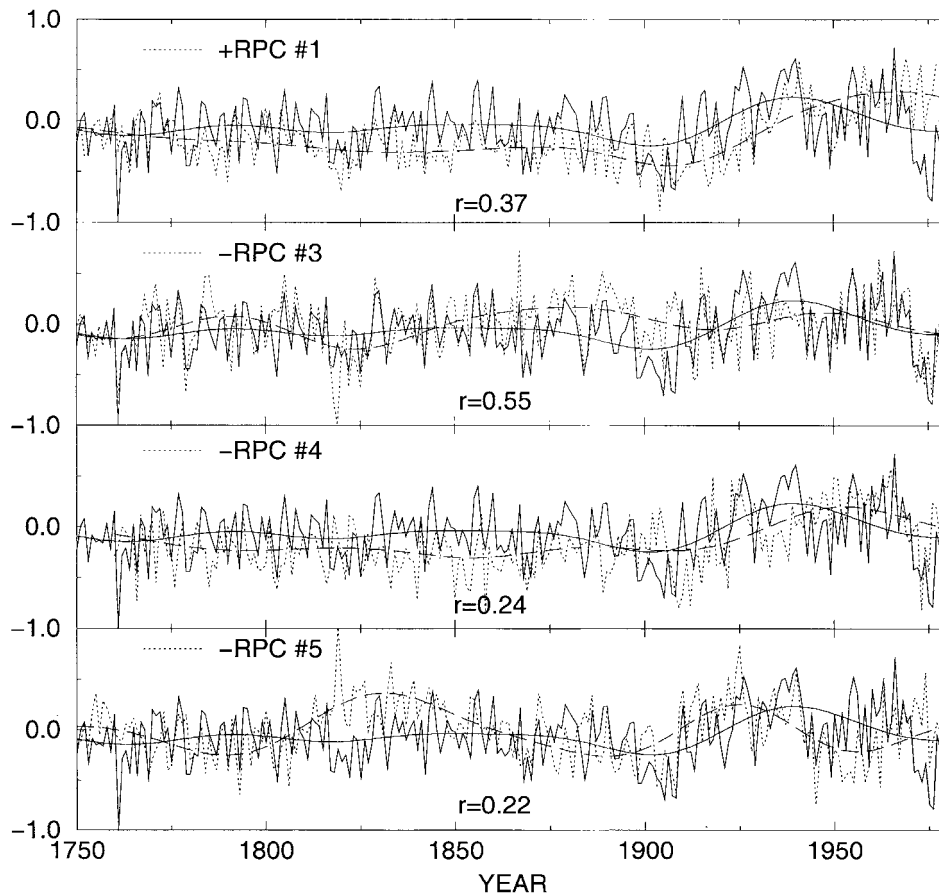


Figure 11. Reconstructed RPCs (dotted) vs. MNET index (solid) back to 1750. The smooth curves highlight the variations on timescales longer than 50 years in the RPC (dashed) and MNET (solid).

It is clear that the NAO-related patterns dominate the behavior in the reconstructed MNET index at interannual timescales (Figure 12). The multidecadal variations in the MNET index are, however, relatively more pronounced than those in the tNAO index (Figure 12). Indeed, other patterns appear to be more important in describing the longer-term MNET variations. A statistically significant relationship between the MNET and reconstructed PC #1 (Figure 11, Table II) arises in large part from the similarity in the low-frequency variations in the two though the mid-20th century (cooling trend late in the 19th century, followed by a warming trend early in the 20th century). The history of the first eigenvector is closely associated with changes in hemispheric mean temperatures. The low-frequency variations therein have been associated largely with solar and volcanic forcing prior to the 20th century, and with anthropogenic greenhouse gas influences during the 20th century (see MBH98). It is interesting that the relationship between this eigen-

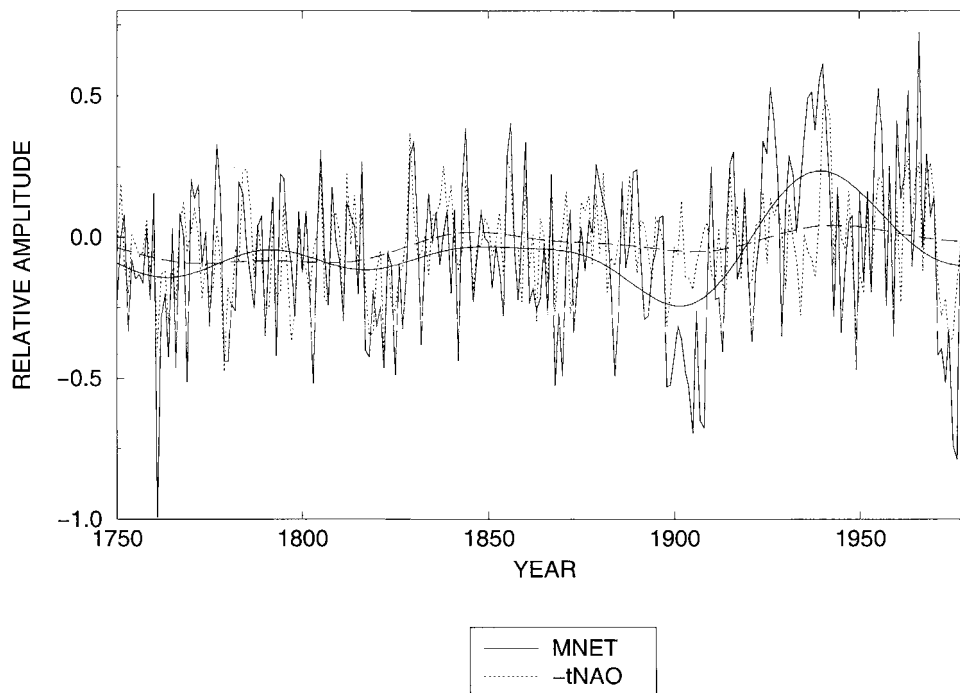


Figure 12. Reconstructed MNET (solid) and tNAO (dotted) indicates back to 1750. The sign of the tNAO index has been reversed to correspond with the sign of its correlation with MNET, and it has been rescaled to have the same variance. The smooth curves highlight the variations on timescales longer than 50 years in the RPC (dashed) and MNET (solid).

vector and MNET temperature trends breaks down in the latter 20th century as the Middle/Near East region cools, while the large-scale warming pattern accelerates. We attribute this breakdown to the relatively weak influence of the global warming pattern on the region (see Figure 2), which is easily overwhelmed by decadal and multidecadal trends in other patterns that more strongly impact on the region.

The recent relative decline in the MNET index results from a combination of recent decadal shifts or trends in the 3rd and 4th eigenvectors. The recent decadal-scale shift in the 3rd eigenvector (PC #3) represents the recent shift in the NAO/tNAO. The recent trend in PC #4, in quadrature with an out-of-phase trend in PC#5, appears to represent the influence of multidecadal (50–70 year period) internal North Atlantic climate processes highlighted by Delworth and Mann (2000, discussed earlier). These multidecadal variations represent a substantial contribution to the low-frequency variability in the MNET index in past centuries, and appear to rival in importance that of the 3rd eigenvector/NAO during the cold-season (see Table II). These relationships are further examined in terms of their frequency-domain attributes (Figure 13). The tNAO and MNET show considerable interannual variability, peaked near 7–8 year period. This peak is clearly evident in the instrumental NAO record (Rogers, 1984), and its robustness back in time is

confirmed by essentially independent dendroclimatic-based NAO reconstructions (Cook et al., 1998). The tNAO spectrum exhibits relatively weak secular variability, in contrast to the MNET index. We attribute this to the greater influence of RPCs #1,4, and 5 on the lowest frequency variability in MNET, as discussed above. In fact, the low-frequency spectrum of the MNET index is most similar to that of RPC #5, strongly peaked at multidecadal timescales of 50–70 year period but statistically insignificant zero-frequency (i.e., long-term trend) variance. This reinforces the early discussion of the importance of the underlying pattern of climate variability on the Middle/Near Eastern region at multidecadal timescales. A relationship between the longer-term modulation of interannual variability in the MNET and tNAO indices is shown through an evolutive spectral analysis of the two time series (Figure 14). Between 1850 and 1900, there is a tendency for lower amplitude low-frequency variability and high-amplitude variations on a roughly 5 year timescale. In contrast, both earlier and later periods show a tendency for higher-frequency interannual variability (3–7) and decadal-scale (7–10 year timescale), and more multidecadal timescale variability. These features are typical of the NAO during the 20th century (see Rogers, 1984; Cook et al., 1998), but this study suggests that they are more variable on century timescales (see also Cook et al., 1998). Interpretation of apparent significant power in the quasibiennial (2.1–2.5 period range) may be compromised by proximity to the Nyquist frequency (0.5 cycle/year) for annual-resolution data.

While we remind the reader that inferences into individual MNET years is limited by the sizeable (60%) fraction of uncalibrated variance in the index, it is nonetheless instructive to examine the large-scale spatial patterns associated with anomalies in the MNET in certain selected years (Figure 15). A number of different factors clearly influence these anomalies during different years. The year 1761, which happens to exhibit warm episode ENSO conditions, also exhibits unusually cold MNET conditions ( $-1.0^{\circ}\text{C}$  anomaly relative to 1902–1980 calibration period mean). This year is associated with one of the (though, not the most) positive reconstructed tNAO index values (index value of 1.30) prior to the 20th century. In contrast, 1777 – La Niña year – happens to be an unusually warm MNET year (anomaly of  $0.33^{\circ}\text{C}$ ), associated with a moderately negative tNAO value (approximately  $-0.2$ ), reinforced by substantial negative loadings on the fifth eigenvector (Figure 10). The ENSO connection in both cases appears coincidental, defying any clear statistical relationship in general, though weak ENSO/NAO relationships have been argued for elsewhere (Rogers, 1984). 1803, one of the few coldest pre-20th century MNET years, is associated with relatively typical values of the tNAO, but an unusually strong loading (see Figure 11) on the 4th EOF (Figure 3), associated with the pattern, as discussed earlier, in which cold-phase ENSO conditions are associated with cold conditions in the Mediterranean and Middle East.

1816, a quite cold year (occurring during an unusually cold decade) for the Northern Hemisphere on the whole (this has been attributed to large-scale cooling due to the Tambora eruption of spring 1815 – see MBH98), is, somewhat

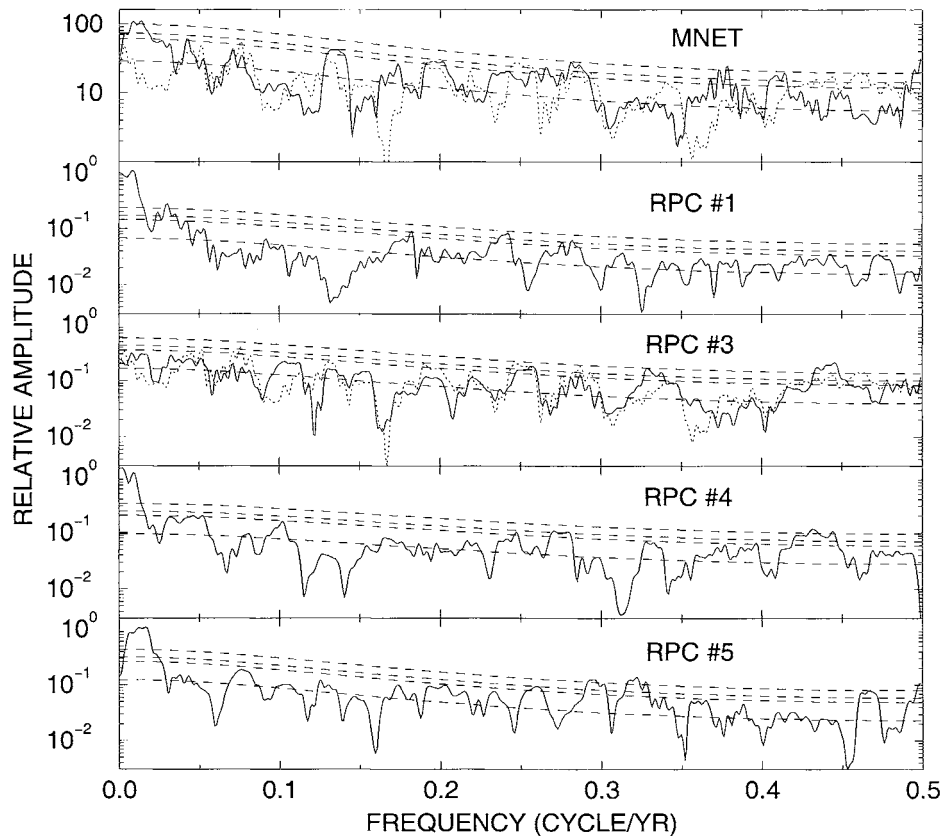
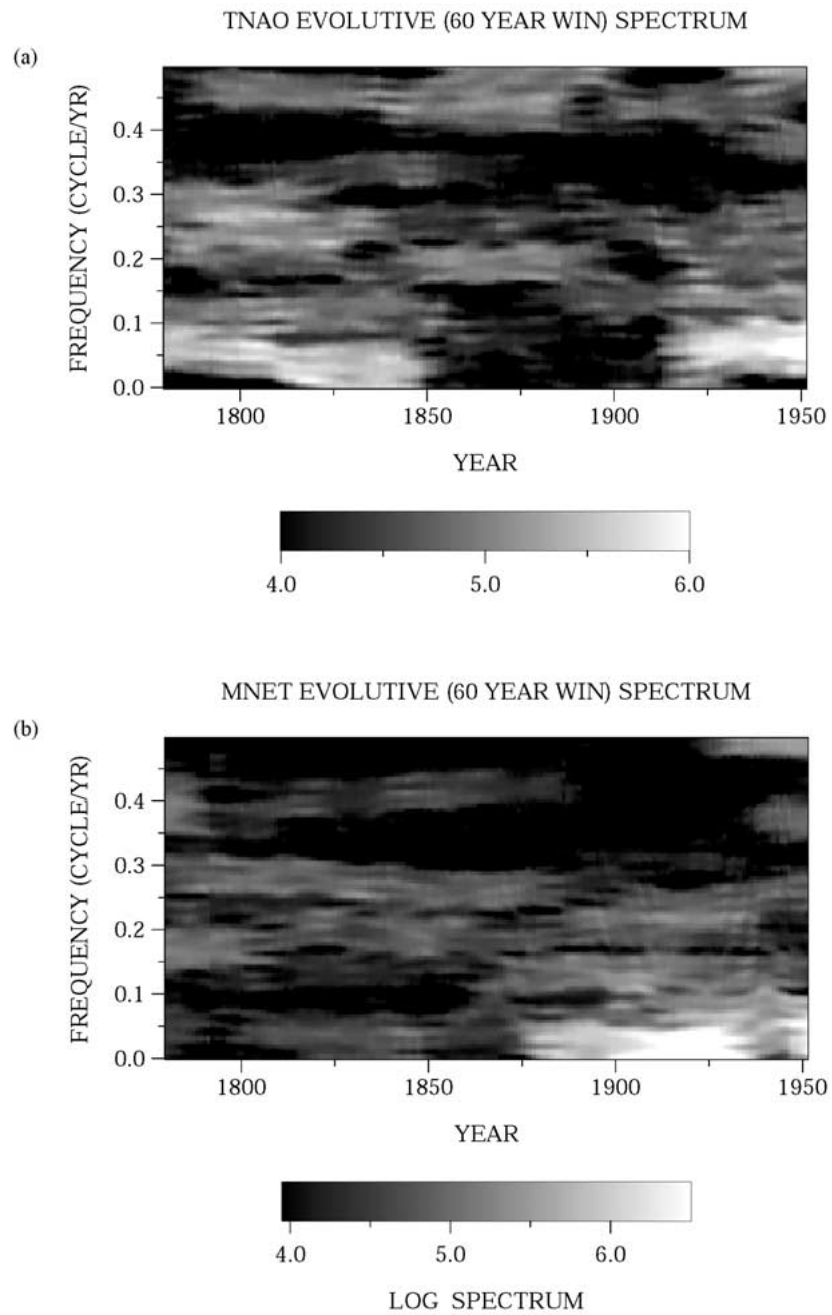


Figure 13. Spectra of various reconstructed PCs and indices each available from 1760–1980. The median, 90%, 95%, and 99% confidence levels relative to the null hypothesis of red noise are shown by the dashed curves. The spectrum and confidence intervals are estimated by the method of Mann and Lees (1996). The spectrum of the reconstructed tNAO index is shown in panels #1 and #3 by the dashed curve, normalized to the same scale shown.

remarkably, an anomalously warm year for the MNET region (anomaly  $0.27^{\circ}\text{C}$ ). This anomaly is associated with a large negative (index =  $-0.30$ ) tNAO anomaly. (The NAO-like temperature pattern for this year has been shown, perhaps not too surprisingly, to be most pronounced during the cold-season [Mann et al., 2000b]). It is interesting to interpret related past studies in this context. For example, the observation by Serre-Bachet et al. (1992) that the Tambora eruption had ‘no effect’ in the western Mediterranean region, reinforced by our own results, can be reinterpreted as resulting from two offsetting effects of the Tambora eruption. One signature of volcanic eruptions appears to be a characteristic NAO-like overprint (e.g., Kelly et al., 1996). Given the effect of the NAO on Mediterranean and Middle/Near Eastern temperatures, we might expect that latter overprint might dominate large-scale cooling associated with negative radiative forcing in this region, leading instead to warming or at least, a lack of cooling. This combination of volcanic influences



*Figure 14.* Evolutionary spectra of (a) reconstructed tNAO and (b) reconstructed MNET indices based on 60 year moving windows. The spectra have been normalized so that any features shown exceed the median red noise level, with lighter shades increasingly more significant. The spectra and confidence levels are estimated by the method of Mann and Lees (1996).

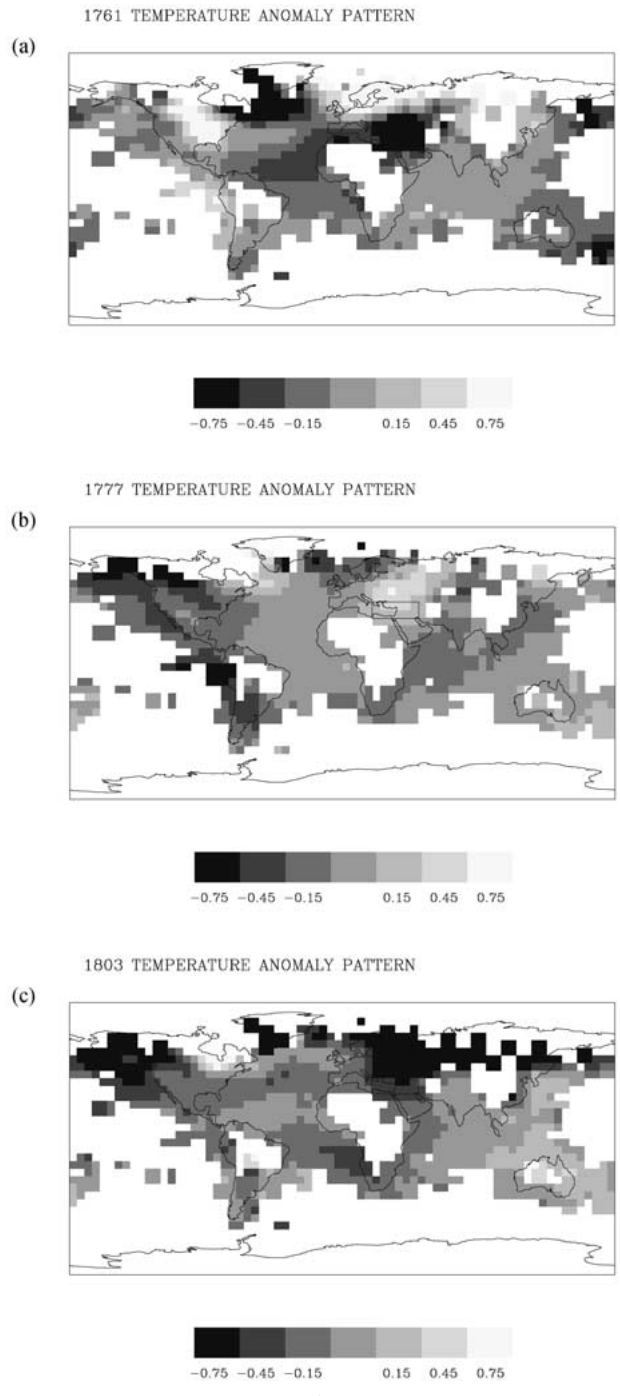


Figure 15a-c.

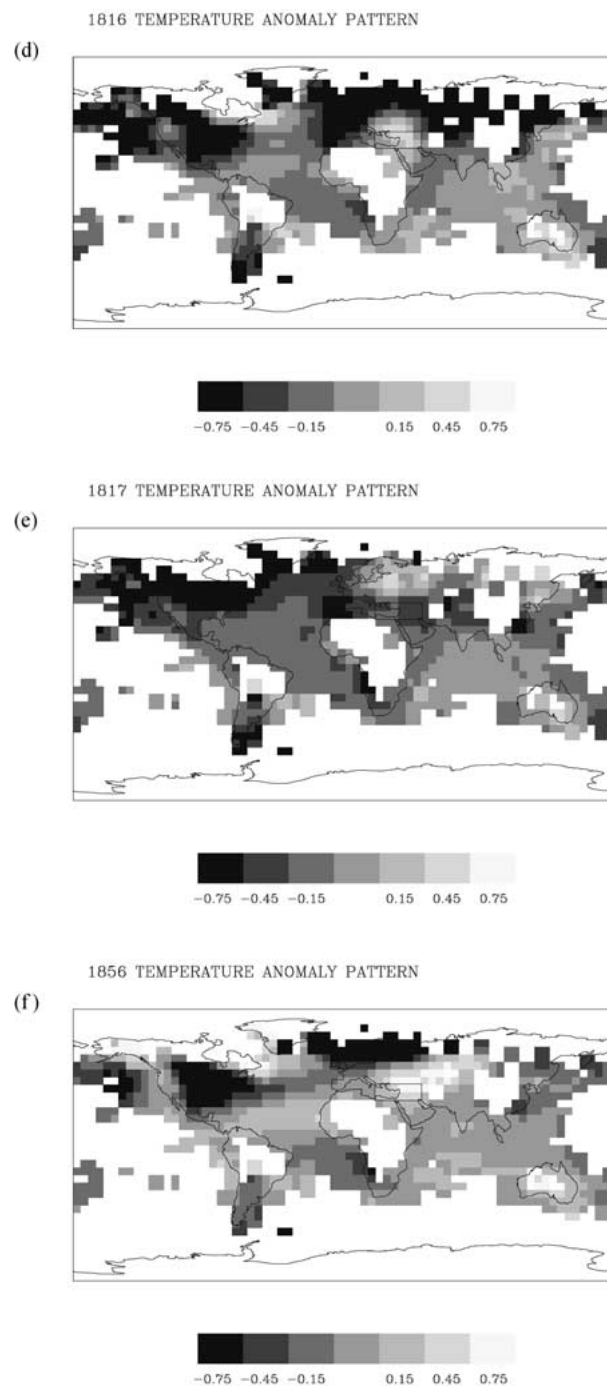


Figure 15d-f.

Figure 15. Large-scale spatial temperature patterns for selected years (a) 1761, (b) 1777, (c) 1803, (d) 1816, (e) 1817, and (f) 1856. The grayscale indicates positive and negative anomalies (in  $^{\circ}\text{C}$ ) relative to the 1902–1980 calibration period mean.

provides a reasonable interpretation of the warming in the Middle/Near East and deficient cooling in western Mediterranean during 1816.

Equally striking, is the transition from 1816 to 1817. 1817 (MNET anomaly =  $-0.40^{\circ}\text{C}$ , tNAO index anomaly = 0.58) represents the first year in a decadal-scale shift to positive phase tNAO and cold MNET conditions. 1856 exhibits the warmest MNET value ( $0.40^{\circ}\text{C}$ ) prior to the 20th century, associated with one of, but not the most, negative reconstructed tNAO index values ( $-0.70$ ) prior to the 20th century. For comparison, 1966 is the warmest MNET value on record ( $0.90^{\circ}\text{C}$ ), while temperatures have since declined in this region during the past couple decades.

## 5. Conclusions

Using a method that combines all of the information available in instrumental, historical, and proxy climate indicators in reconstructing annual and seasonal patterns of temperature back through the mid-18th century, we have assessed, as best currently possible, the apparent patterns of large-scale climate variation during the past few centuries, and their relationship to past temperature variations in the Middle and Near East. From this assessment, interannual temperature variability in the region appears to be closely related to patterns of variation associated with the NAO. Changes in the amplitude and dominant timescale of the NAO appear largely responsible for similar variations in middle and near eastern temperatures in the past centuries on interannual and decadal timescales. Other patterns, however, appear to be more important on multidecadal and secular timescales. Increasing temperatures in the region during the early 20th century appear to be related to the modest but not-insignificant projection of an overall global warming pattern on the region. However, an overprint of cooling in the region during recent decades appears to be related to other patterns which have a prominent influence on the region, and overwhelm the weaker influence of the global warming pattern on this region. This includes recent trends in the NAO itself but as, or more, importantly, distinct multidecadal patterns of climate influencing the Atlantic and neighboring land regions. One important consequence of these observations is the possibility that natural variability has masked the influence of possible anthropogenic climate forcing in the past, but will not mask stronger projected trends in the future (IPCC, 1996). Understanding both the patterns of natural variability and possible influences of anthropogenic forcing is particularly important in this climatically stressed, societally-volatile region.

## Acknowledgements

The climate reconstructions analyzed in this paper resulted from collaboration with R. S. Bradley and M. K. Hughes, whose contributions to making the current work

possible are gratefully acknowledged. I am also grateful to Frank Keimig for technical assistance. This manuscript benefited greatly from the helpful comments of J. Guiot, and an anonymous reviewer. This work was supported by the Alexander Hollaender Distinguished Postdoctoral Research Fellowship program of the Department of Energy, and the NSF- and NOAA-sponsored Earth Systems History Program (NSF ATM-9626833 and NOAA NA96GP0404).

### References

- Appenzeller, C., Schwander, J., Sommer, S., and Stocker, T. F.: 1998, 'The North Atlantic Oscillation and its Imprint on Precipitation and Ice Accumulation in Greenland', *Geophys. Res. Lett.* **25**, 1939–1942.
- Barnett, T. P., Santer, B., Jones, P. D., Bradley, R. S., and Briffa, K. R.: 1996, 'Estimates of Low Frequency Natural Variability in Near-Surface Air Temperature', *Holocene* **6**, 255–263.
- Bradley, R. S. and Jones, P. D.: 1993, '“Little Ice Age” Summer Temperature Variations: Their Nature and Relevance to Recent Global Warming Trends', *Holocene* **3**, 367–376.
- Cane, M. A., Clement, A. C., Kaplan, A., Kushnir, Y., Pozdnyakov, D., Seager, R., Zebiak, S. E., and Murtugudde, R.: 1997, 'Twentieth-Century Sea Surface Temperature Trends', *Science* **275**, 957–960.
- Cole, J. E. and Cook, E. R.: 1998, 'The Changing Relationship between ENSO Variability and Moisture Balance in the Continental United States', *Geophys. Res. Lett.* **25**, 4529–4532.
- Cook, E., D'Arrigo, R. D., and Briffa, K. R.: 1998, 'A Reconstruction of the North Atlantic Oscillation Using Tree-Ring Chronologies from North America and Europe', *Holocene* **8**, 9–17.
- Cullen, H., D'Arrigo, R., Cook, E., and Mann, M. E.: 2001, 'Multiproxy-Based Reconstructions of the North Atlantic Oscillation over the Past Three Centuries', *Paleoceanography* **15**, 27–39, 2001.
- Cullen, H., Kaplan, A., Arkin, P. A. and deMenocal, P. B.: 2002, 'Impact of the North Atlantic Oscillation on Middle Eastern Climate and Streamflow', *Clim. Change*, this issue.
- Crowley, T. J. and Kim, K. Y.: 1996, 'Comparison of Proxy Records of Climate Change and Solar Forcing', *Geophys. Res. Lett.* **23**, 359–362.
- D'Arrigo, R., Cook, E. R., and Cullen, H.: 1997, 'North Atlantic Sector Tree-Ring Records and SST Variability', *NOAA Atlantic Climate Change Program (ACCP) Notes* **4**, 1–5.
- D'Arrigo, R. D., Cook, E. R., Jacoby, G. C., and Briffa, K. R.: 1993, 'NAO and Sea Surface Temperature Signatures in Tree-Ring Records from the North Atlantic Sector', *Quat. Sci. Rev.* **12**, 431–440.
- Delworth, T. D., Manabe, S., and Stouffer, R. J.: 1993, 'Interdecadal Variations of the Thermohaline Circulation in a Coupled Ocean-Atmosphere Model', *J. Climate* **6**, 1993–2011.
- Delworth, T. D., Manabe, S., and Stouffer, R. J.: 1997, 'Multidecadal Climate Variability in the Greenland Sea and Surrounding Regions: A Coupled Model Simulation', *Geophys. Res. Lett.* **24**, 257–260.
- Delworth, T. D. and Mann, M. E.: 2000, 'Observed and Simulated Multidecadal Variability in the North Atlantic', *Clim. Dyn.* **16**, 661–676.
- Folland, C. K., Parker, D. E., and Kates, F. E.: 1984, 'Worldwide Marine Temperature Fluctuations 1856–1981', *Nature* **310**, 670–673.
- Halpert, M. S. and Ropelewski, C. F.: 1992, 'Surface Temperature Patterns Associated with the Southern Oscillation', *J. Climate* **5**, 577–593.
- Heiss, G. A.: 1994, *Coral Reefs in the Red Sea: Growth, Production and Stable Isotopes*, GEOMAR Report 32, pp. 1–141.

- Hughes, M. K. and Diaz, H. F.: 1994, 'Was There a "Medieval Warm Period" and if So, Where and When?', *Clim. Change* **26**, 109–142.
- Hurrell, J. W.: 1995, 'Decadal Trends in the North Atlantic Oscillation, Regional Temperatures and Precipitation', *Science* **269**, 676–679.
- Intergovernmental Panel on Climate Change (IPCC): 1996, 'Climate Change 1995', in Houghton, J. T. et al. (eds.), *The Science of Climate Change*, Cambridge University Press, Cambridge.
- Jones, P. D. and Briffa, K. R.: 1992, 'Global Surface Air Temperature Variations during the 20th Century: Part 1 – Spatial, Temporal and Seasonal Details', *Holocene* **1**, 165–179.
- Jones, P. D., Briffa, K. R., Barnett, T. P., and Tett, S. F. B.: 1998, 'High-Resolution Paleoclimatic Records for the Last Millennium: Interpretation, Integration and Comparison with General Circulation Model Control Run Temperatures', *Holocene* **8**, 477–483.
- Jones, P. D., Jonsson, T., and Wheeler, D.: 1997, 'Extension to the North Atlantic Oscillation Using Early Instrumental Pressure Observations from Gibraltar and South-West Iceland', *Int. J. Clim.* **17**, 1433–1450.
- Jones, P. D., New, M., Parker, D. E., Martin, S., and Rigor, J. G.: 1999, 'Surface Air Temperature and its Changes over the Past 150 Years', *Rev. Geophys.* **37**, 173–199.
- Kelly, P. M., Jones, P. D., and Pengqun, J.: 1996, 'The Spatial Response of the Climate System to Explosive Volcanic Eruptions', *Int. J. Clim.* **16**, 537–550.
- Kushnir, Y.: 1994, 'Interdecadal Variations in North Atlantic Sea Surface Temperature and Associated Atmospheric Conditions', *J. Climate* **7**, 141–157.
- Lean, J., Beer, J., and Bradley, R. S.: 1995, 'Reconstruction of Solar Irradiance Since 1610: Implications for Climate Change', *Geophys. Res. Lett.* **22**, 3195–3198.
- Mann, M. E., Bradley, R. S., and Hughes, M. K.: 1998, 'Global-Scale Temperature Patterns and Climate Forcing over the Past Six Centuries', *Nature* **392**, 779–787.
- Mann, M. E., Bradley, R. S. and Hughes, M. K.: 1999, 'Northern Hemisphere Temperatures During the Past Millennium: Inferences, Uncertainties, and Limitations', *Geophys. Res. Lett.* **26**, 759–762.
- Mann, M. E., Bradley, R. S., and Hughes, M. K.: 2000a, 'Long-Term Variability in the El Niño Southern Oscillation and Associated Teleconnections', in Diaz, H. F. and Markgraf, V. (eds.), *El Niño and the Southern Oscillation: Multiscale Variability and its Impacts on Natural Ecosystems and Society*, Cambridge University Press, Cambridge, U.K., 357–412.
- Mann, M. E., Gille, E., Bradley, R. S., Hughes, M. K., Overpeck, J. T., Keimig, F.T., and Gross, W.: 2000b, 'Annual Temperature Patterns in Past Centuries: An Interactive Presentation', *Earth Interact.* **4-4**, 1–29.
- Mann, M. E. and Lees, J.: 1996, 'Robust Estimation of Background Noise and Signal Detection in Climatic Time Series', *Clim. Change* **33**, 409–445.
- Mann, M. E. and Park, J.: 1994, 'Global-Scale Modes of Surface Temperature Variability on Interannual to Century Timescales', *J. Geophys. Res.* **99**, 25819–25833.
- Mann, M. E. and Park, J.: 1996, 'Joint Spatiotemporal Modes of Surface Temperature and Sea Level Pressure Variability in the Northern Hemisphere during the Last Century', *J. Climate* **9**, 2137–2162.
- Mann, M. E., Park, J., and Bradley, R. S.: 1995, 'Global Interdecadal and Century-Scale Oscillations during the Past Five Centuries', *Nature* **378**, 266–270.
- Overpeck, J., Hughen, K., Hardy, D., Bradley, R., Case, R., Douglas, M., Finney, B., Gajewski, K., Jacoby, G., Jennings, A., Lamoureux, S., Lasca, A., Macdonald, G., Moore, J., Retelle, M., Smith, S., Wolfe, A., and Zielinski, G.: 1997, 'Arctic Environmental Changes of the Last Four Centuries', *Science*, 1251–1256.
- Price, C., Stone, L., Huppert, A., Rajagopalan, B., and Alpert, P.: 1998, 'A Possible Link between El Niño and Precipitation in Israel', *Geophys. Res. Lett.* **25**, 3963–3966.
- Rogers, J. C.: 1984, 'The Association between the North Atlantic Oscillation and the Southern Oscillation in the Northern Hemisphere', *Mon. Wea. Rev.* **112**, 1999–2015.

- Ropelewski, C. F. and Halpert, M. S.: 1987, 'Global and Regional Scale Precipitation Patterns Associated with the El Niño/Southern Oscillation', *Mon. Wea. Rev.* **115**, 1606–1626.
- Schlesinger, M. E. and Ramankutty, N.: 1994, 'An Oscillation in the Global Climate System of Period 65–70 Years', *Nature* **367**, 723–726.
- Serre-Bachet, F., Guiot, J., and Tessier, L.: 1992, 'Dendroclimatic Evidence from Southwestern Europe and Northwestern Africa', in Bradley, R. S. and Jones, P. D. (eds.), *Climate since A. D. 1500*, Routledge, London, pp. 349–365.
- Shindell, D. T., Miller, R. L., Schmidt, G. A., and Pandolfo, L.: 1999, 'Simulation of Recent Northern Winter Climate Trends by Greenhouse-Gas Forcing', *Nature* **399**, 452–455.
- Tourre, Y. M., Rajagopalan, B., and Kushnir, Y.: 1998, 'Dominant Patterns of Climate Variability in the Atlantic Ocean Region during the Last 136 Years', *J. Climate* **12**, 2285–2299.
- Waple, A., Mann, M. E., and Bradley, R. S.: 2000, 'Long-Term Patterns of Solar Irradiance Forcing in Model Experiments and Proxy-Based Surface Temperature Reconstructions', *Clim. Dyn.*, accepted.

(Received 7 October 1999; in revised form 26 December 2001)